Terrestrial Aridity and Its Response to Greenhouse Warming across CMIP5 Climate Models

JACOB SCHEFF AND DARGAN M. W. FRIERSON

Department of Atmospheric Sciences, University of Washington, Seattle, Washington

(Manuscript received 8 July 2014, in final form 16 April 2015)

ABSTRACT

The aridity of a terrestrial climate is often quantified using the dimensionless ratio P/PET of annual precipitation (P) to annual potential evapotranspiration (PET). In this study, the climatological patterns and greenhouse warming responses of terrestrial P, Penman–Monteith PET, and P/PET are compared among 16 modern global climate models. The large-scale climatological values and implied biome types often disagree widely among models, with large systematic differences from observational estimates. In addition, the PET climatologies often differ by several tens of percent when computed using monthly versus 3-hourly inputs.

With greenhouse warming, land P does not systematically increase or decrease, except at high latitudes. Therefore, because of moderate, ubiquitous PET increases, P/PET decreases (drying) are much more widespread than increases (wetting) in the tropics, subtropics, and midlatitudes in most models, confirming and expanding on earlier findings. The PET increases are also somewhat sensitive to the time resolution of the inputs, although not as systematically as for the PET climatologies.

The changes in the balance between P and PET are also quantified using an alternative aridity index, the ratio $P/(P + \text{PET})$, which has a one-to-one but nonlinear correspondence with P/PET. It is argued that the magnitudes of $P/(P + \text{PET})$ changes are more uniformly relevant than the magnitudes of P/PET changes, which tend to be much higher in wetter regions. The ratio $P/(P + \text{PET})$ and its changes are also found to be excellent statistical predictors of the land surface evaporative fraction and its changes.

1. Introduction

Our everyday experience tells us that precipitation (P) is one of the factors that determines the effective wetness or dryness of a terrestrial climate, but not the only one. For example, the ''emerald city'' of Seattle, Washington, receives $\sim$950 mm yr^{-1} of P on average. Yet the environment of Dallas, Texas, which also averages $\sim$950 mm yr^{-1} of P, seems much drier. This is because its more intense sunshine and warmer, drier air evaporate plant and soil water more effectively.

Therefore, when characterizing climatic aridity, it makes sense to consider P relative to potential evapotranspiration (PET; e.g., Hartmann 1994), the rate at which the climate demands water from well-watered vegetation. PET is best computed from climate data using the Penman–Monteith equation (see section 2), which is just the solution to the physical equations for the energy balance that would hold over a wet surface in given climatic conditions (e.g., Monteith 1981; Allen et al. 1998, 2005). According to one standard dataset (FAO 2004), PET in Seattle is $\sim$840 mm yr^{-1}, but PET in Dallas is $\sim$1560 mm yr^{-1}, far more water than can actually be supplied by P. Of course, an extensive wet area would cool and moisten those climatic conditions, lowering the PET estimates, but plants in a given environment experience its actual (hot, dry) climate, so for ecological purposes it is sensible to use the actual climate when computing PET. The concept of PET is also known as reference evapotranspiration, potential evaporation, or evaporative demand, and is very closely related to pan evaporation.

The simplest measure that accounts for the relative magnitudes of P and PET is the ratio of their climatological annual mean values, the aridity index P/PET (e.g., Transeau 1905; Budyko and Miller 1974; Middleton and Thomas 1997; Feng and Fu 2013), which can be thought of as a nondimensionalized precipitation. The value of P/PET indicates whether evapotranspiration should be

Corresponding author address: Jacob Scheff, Lamont-Doherty Earth Observatory, 301F Oceanography, 61 Route 9W, P.O. Box 1000, Palisades, NY 10964.
E-mail: jscheff@ldeo.columbia.edu

DOI: 10.1175/JCLI-D-14-00480.1

TABLE 1. CMIP5 models analyzed in this study.

Model acronym	Expansion
ACCESS1.0[a]	Australian Community Climate and Earth-System Simulator version 1.0
BCC-CSM1.1	Beijing Climate Center (BCC) Climate System Model version 1.1, low resolution
BCC-CSM1.1(m)	BCC Climate System Model version 1.1, medium resolution
BNU-ESM	Beijing Normal University–Earth System Model
CNRM-CM5	Centre National de Recherches Météorologiques (France) Coupled Global Climate Model, version 5
GFDL-CM3	NOAA Geophysical Fluid Dynamics Laboratory (GFDL) Climate Model, version 3
GFDL-ESM2G	GFDL Earth System Model with Generalized Ocean Layer Dynamics (GOLD) component
GFDL-ESM2M	GFDL Earth System Model with Modular Ocean Model (MOM), version 4 component
GISS-E2-H[b,c]	NASA Goddard Institute for Space Studies (GISS) Model E2, coupled with Hybrid Coordinate Ocean Model (HYCOM)
GISS-E2-R[b,c]	GISS Model E2, coupled with the Russell ocean model
HadGEM2-ES[a,d,e]	Met Office Hadley Centre (UK) Global Environment Model version 2–Earth System
INM-CM4	Institute for Numerical Mathematics (Russia) Coupled Model version 4
IPSL-CM5A-LR	L'Institut Pierre-Simon Laplace (IPSL; France) Coupled Model, version 5a, low resolution
IPSL-CM5A-MR	IPSL, Coupled Model, version 5a, medium resolution
MRI-CGCM3	Meteorological Research Institute (MRI; Japan) Coupled Atmosphere–Ocean General Circulation Model, version 3
MRI-ESM1	MRI Earth System Model, version 1

[a] Surface winds were given on a grid staggered from that of the other surface variables; see the appendix of SF14.
[b] Version with interactive aerosols and chemistry ("p3") is shown here; results for version with prescribed aerosols and chemistry ("p1") were nearly identical.
[c] Run 6 was used for historical and run 2 was used for RCP8.5, as these were the only respective runs with 3-hourly output.
[d] Run 2 was used for historical (and run 1 was used for RCP8.5), as these were the only respective runs with 3-hourly output.
[e] 3-hourly surface pressure was not available, so monthly surface pressure output was used for each 3-h interval.

water-limited ($P \ll$ PET) or energy-limited ($P \gg$ PET), and a difference in P/PET between two climates implies a difference in limiting-factor importance. From the above data, P/PET is ~1.13 in Seattle, but only ~0.61 in Dallas. Budyko and Miller (1974) and earlier workers noted that the same values of P/PET correspond to similar vegetation densities and runoff ratios across widely varying temperature, radiation, and PET regimes on Earth. This observation has led to the use of P/PET as the main moisture variable in several prominent terrestrial biome classification schemes (e.g., Middleton and Thomas 1997; Holdridge 1967). In the Middleton and Thomas (1997) scheme, which has been adopted by the United Nations (UN; e.g., Mortimore 2009), P/PET < 0.05 is defined as hyperarid, $0.05 < P$/PET < 0.2 as arid, $0.2 < P$/PET < 0.5 as semiarid, $0.5 < P$/PET < 0.65 as dry subhumid, and P/PET > 0.65 as humid. The climate of Dallas is thus dry subhumid while that of Seattle is quite humid, even though P is the same.

Global climate models (GCMs) are often used to generate hydroclimatic responses to various forcings. However, these responses have usually been characterized in terms of individual dimensional quantities such as P, actual evapotranspiration (E or ET), runoff, and/or soil moisture (e.g., Collins et al. 2014; Meehl et al. 2007), or in terms of complicated metrics of local drought relative to some reference period, such as the Palmer drought severity index (PDSI) (Cook et al. 2014; Dai 2013). The characterization of the models' mean states has been similarly concerned with individual variables, and has often focused on features over the oceans, especially for P (e.g., Flato et al. 2014). In contrast, very few studies have tried to quantify the patterns of general land aridity in climate models, or of the response of aridity to forcing. Here we propose to build on the work of Feng and Fu (2013) by mapping P/PET, its response to greenhouse warming, and its contributing factors across a wide range of modern GCMs over global land.

2. Methods

Given values of near-surface air temperature T_a, water vapor pressure e_a, wind speed $|u|$, and net downward broadband radiation R_n, the Penman–Monteith equation for PET is

$$\mathrm{PET} = \left[\frac{\Delta(R_n - G) + \rho_a c_p (e^* - e_a) C_H |u|}{\Delta + \gamma(1 + r_s C_H |u|)}\right] \Big/ L_v, \qquad (1)$$

where e^* is the saturation vapor pressure at T_a, $\Delta = de^*/dT(T_a)$ is a standard notation for the local *slope* of the saturation vapor pressure curve, r_s is the assumed bulk stomatal resistance of well-watered vegetation, C_H is an assumed scalar transfer coefficient, ρ_a is the air density, c_p is the air specific heat, L_v is the heat of vaporization of water, $\gamma = (c_p p_s)/(\varepsilon L_v)$,

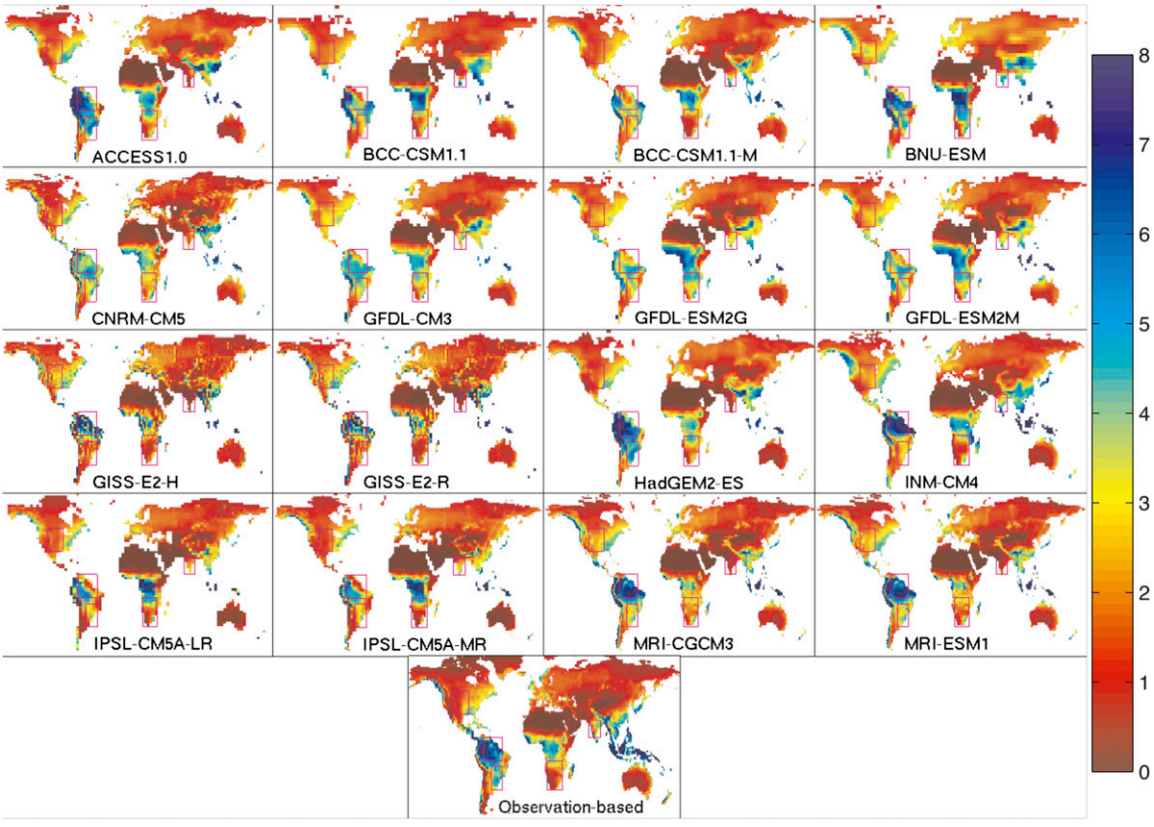

FIG. 1. 1981–99 climatological annual-mean precipitation P in mm day^{-1} for each CMIP5 model in Table 1, with Global Precipitation Climatology Centre (GPCC) gauge-based observational product as described in section 2. Values in a few color-saturated regions greatly exceed those on the scale. Regions in Table 2 are outlined.

p_s is the air pressure, $\varepsilon \approx 0.622$ is the ratio of molar masses of water vapor and dry air, and G is the heat flux into the ground or soil (usually ignored or parameterized).

In a previous study (Scheff and Frierson 2014, hereinafter SF14), the authors computed 1981–99 and 2081–99 annual PET climatologies for 13 GCMs in phase 5 of the Coupled Model Intercomparison Project (CMIP5) multimodel ensemble (Taylor et al. 2012), using 3-hourly surface output from the historical and business-as-usual RCP8.5 scenarios in a procedure closely adapted from the American Society of Civil Engineers' (ASCE) standardized tall-crop version of (1) for hourly data (Allen et al. 2005). Here we make use of those same PET climatologies, expanded to include the three additional CMIP5 GCMs that have since archived output satisfying the SF14 criteria. The resulting 16 models are listed in Table 1 along with any exceptions to the SF14 procedures. Note that the GCM's land surface skin temperature T_s (as opposed to T_a) is not used in (1); instead, the derivation of (1) uses the often much cooler skin temperature of a wet surface, consistent with the definition of PET. Thus, the conceptual problem with GCM internal "PET" fields identified by Milly (1992) is explicitly avoided by using the Penman–Monteith approach. See Milly (1992) and section 1b of SF14.

In addition, we apply the SF14 procedures to 3-hourly, 1°, 1981–99 meteorological data from the Global Land Data Assimilation System 2.0 (GLDAS; Rodell et al. 2004) to obtain a comparable observational estimate of climatological PET. These data come directly from the widely used Sheffield et al. (2006) meteorological forcing dataset, except for the upward energy fluxes used to compute ($R_n - G$), which inevitably have some influence from the Noah land model used in GLDAS.

TABLE 2. Region definitions.

Northern South America	10°S–10°N, 45°–70°W
Southeast South America	35°–15°S, 45°–60°W
Central North America	30°–50°N, 90°–110°W
Indian Peninsula	10°–25°N, 70°–85°E
Southern Africa	35°–10°S, 15°–35°E

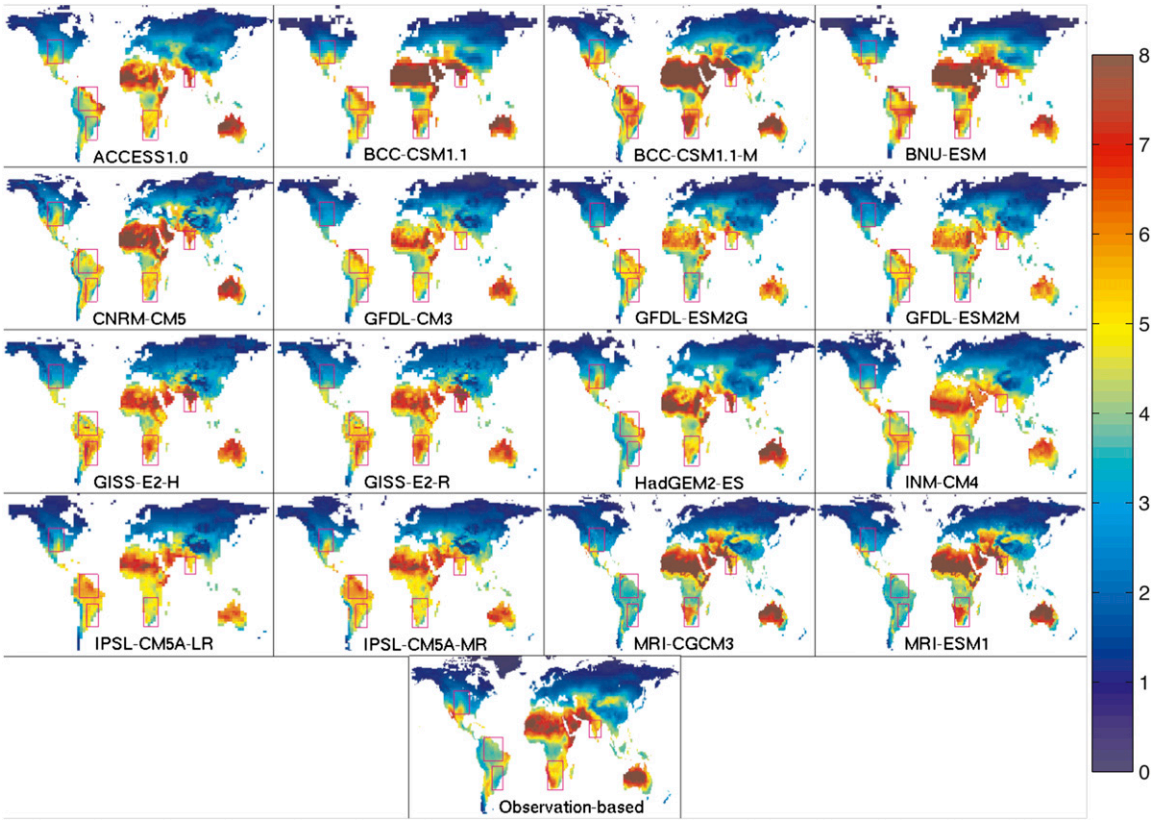

FIG. 2. 1981–99 annual-mean potential evapotranspiration (PET) in mm day^{-1} for each model and for the Global Land Data Assimilation System 2.0 (GLDAS) observation-based product as described in section 2.

We also compute all of these PET climatologies using monthly-mean instead of 3-hourly output, with a procedure closely adapted from the ASCE standardized tall-crop version of (1) for daily data. This is very similar to the 3-hourly SF14 procedure; the main differences (after Allen et al. 2005) are that e^* is estimated as the average of $e^*(T_{min})$ and $e^*(T_{max})$, where T_{min} and T_{max} are the monthly-mean daily minimum and maximum values of T_a; that Δ is somewhat differently estimated as $\Delta(T_{mean})$, where T_{mean} is the average of T_{min} and T_{max}; and that r_s is set to a constant 45 s m^{-1}. (The only other difference is that the monthly average of $|u|$ is archived directly by the models as the variable sfcWind, not computed from the vector components.) This is much less computationally intensive than using 3-hourly output, and many previous studies (e.g., Feng and Fu 2013; Cook et al. 2014; Dai 2013) have also used monthly-mean output, so the comparison is of considerable interest. However, contrary to their stated method (Allen et al. 1998) and to Allen et al. (2005), those studies simply estimated e^* as $e^*(T_{mean})$, so we also do another set of monthly PET computations using this nonstandard e^* estimate for comparison to our main results. (For the GLDAS observations, we *only* use this nonstandard method, since T_{min} and T_{max} are not included in the GLDAS monthly product.)

Finally, P (unlike PET) is one of the variables directly saved by the GCMs, so we compute its annual climatologies using monthly-mean output, for simplicity. We also use gauge-based observational estimates from the Global Precipitation Climatology Centre (GPCC) 1951–2000 climatology product (Schneider et al. 2014), for comparison. [The 1981–99 mean of the less comprehensive Climatic Research Unit TS3.21 P product (Harris et al. 2014) is nearly identical.]

3. Results and discussion

a. Basic states

Figure 1 maps the 1981–99 terrestrial P climatologies for each GCM in Table 1, with the GPCC observational product also shown for reference and five key regions (defined in Table 2) outlined with rectangles. One can immediately see that while in many places the models are quite similar to each other and to the observations

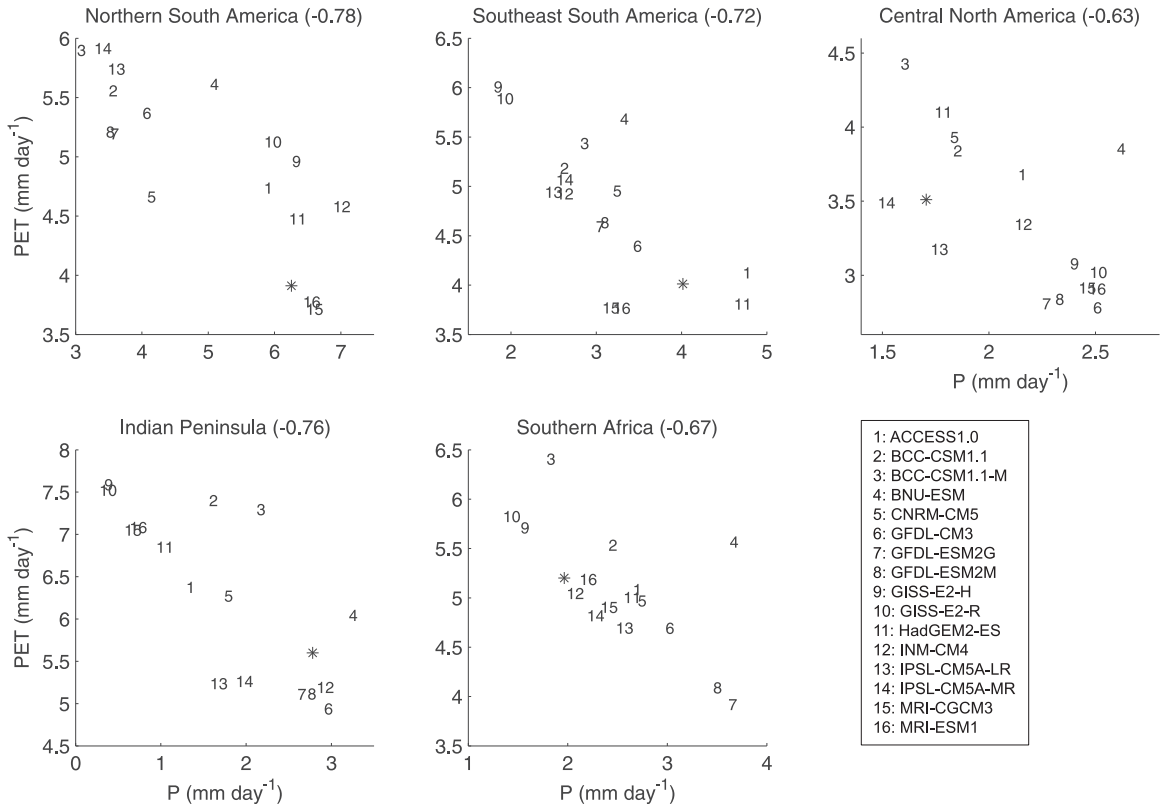

FIG. 3. 1981–99 annual-mean regional-land-mean P vs PET for each model (numbers) and for the observational products (asterisks), plotted for each region in Table 2. Values in parentheses are simple correlations of the 16 model points.

(e.g., much of Eurasia and northern Africa), in many other places they differ greatly. Perhaps the most dramatic model-to-model differences are in the outlined region of northern South America (as well as neighboring Central America), where many models simulate only 1–2 mm day^{-1} of precipitation (red and orange, similar to the Sahel or the interior western United States) across the same vast areas where other models (and the observations) have 5–8 mm day^{-1} or more (blue), and dense tropical rain forests are found. The same situation, where some models have near-observed large-scale P but other models have a great deal less, also occurs across the central Amazon basin and the (outlined) southeast of the continent; Malhi et al. (2009) noted similar behavior in the CMIP3 models. This type of difference is also particularly stark for the Indian Peninsula (also outlined), where some models have 0–1 mm day^{-1} yet most other models (and the observations) have 3 mm day^{-1}. Conversely, through large portions of southern Africa (outlined) and central Africa, several models simulate roughly double the observed P amounts, while many other models are closer to observed. Southern and central China and much of central North America (outlined) also have striking intermodel P disagreements.

Figure 2 shows the corresponding climatologies of annual Penman–Monteith PET (computed using the 3-hourly output) on the same scale. (This is simply an expansion and rescaling of SF14's Fig. 1, plus an observational panel.) In many of the same low- to midlatitude areas where the models strongly disagree on P, they also strongly disagree on PET, and the high-P models are often also the low-PET models in a given area. For example, in much of South America, the two MRI models (and ACCESS1.0 and HadGEM2-ES to a lesser extent; see Table 1 for model expansions), which all showed high, realistic P in Fig. 1, also have much lower, more realistic PET, just 3–4 mm day^{-1} (light blue) where most of the other models have 5–7 mm day^{-1} (yellow to red), much greater than observed. Similar patterns of very large, opposite biases in PET and P are also common in the southern African and Indian peninsular regions. This negative intermodel relationship is somewhat to be expected, since rainier simulated climates also likely have less sunshine, higher relative humidity, and (in the tropics and/or warm seasons) cooler daytime temperatures, all of which mean lower Penman–Monteith PET

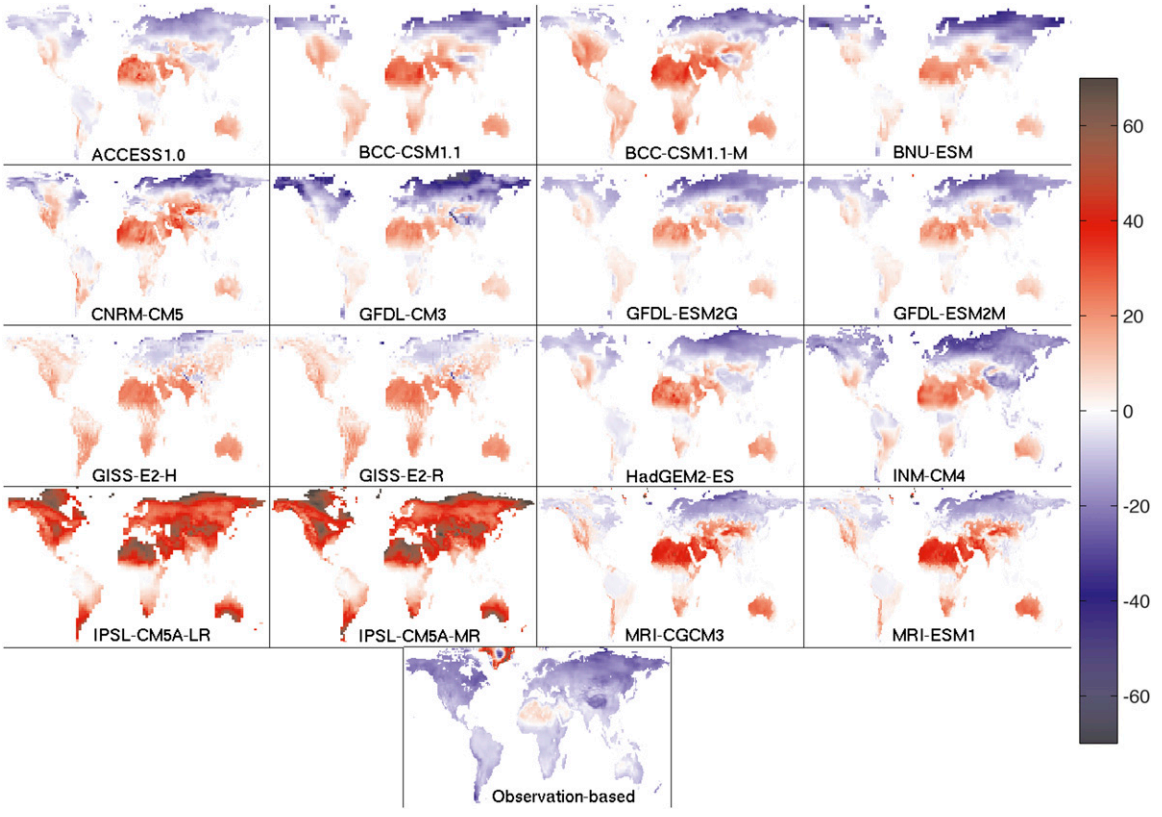

FIG. 4. Percent differences between the 1981–99 annual-mean PET computed using monthly vs 3-hourly output, for each model and for the GLDAS observation-based product. For the observations only, the nonstandard $e^* = e^*(T_{mean})$ is used in the monthly computation.

(e.g., Allen et al. 2005; SF14; see also Brutsaert and Parlange 1998). However, there are also strong PET intermodel differences in Fig. 2 that do not show such a clear association with P differences. For example, maximum PET values in the central Sahara, where $P \sim 0$, range from 6 to over 8 mm day^{-1} (Fig. 1 of SF14 shows that some of these models exceed 10 mm day^{-1}, in fact).

Figure 3 distills these relationships by taking area-weighted means of Figs. 1 and 2 over all land in each region, and plotting the regional P and PET against each other. (These means are taken by nearest-neighbor interpolating each model onto a common 0.25° grid and using only those 0.25° grid points which get assigned to an analyzed grid box for *every* model, so that the same set of points is used in each model despite the different coastlines.) The negative intermodel relationship between mean-state P and PET is always visually clear, and the correlation is always stronger than −0.6. The dramatic, zeroth-order differences between many models and the observational estimates are also made clear: some models have barely half observed P for the two South American regions (or nearly twice observed P for the southern African region) and/or an order of magnitude less P than observed for the Indian peninsular region. The large scale of the defined regions means that somewhat smaller-scale differences (e.g., across the north coast of South America) are even greater.

Figure 4 shows the percent differences between the Penman–Monteith PET climatologies computed using monthly-mean output (with the standard e^* estimate) and those computed using 3-hourly output just shown in Fig. 2. Throughout much of the low- to midlatitudes the monthly-computed PET is higher than the 3-hourly value by about 10%–30%, with the exact magnitude and extent of the difference varying somewhat among models. At high latitudes the difference typically takes the opposite sign and is somewhat smaller. (In the two IPSL models, the discrepancy is much larger and consistently positive.) The discrepancy turns out to be largely explained by a rather uniform 20%–50% (50%–150% in the IPSL models) overestimation of the aerodynamic (i.e., right hand) term of Eq. (1) by the monthly method. Similar magnitude discrepancies, albeit with different signs and patterns, are found

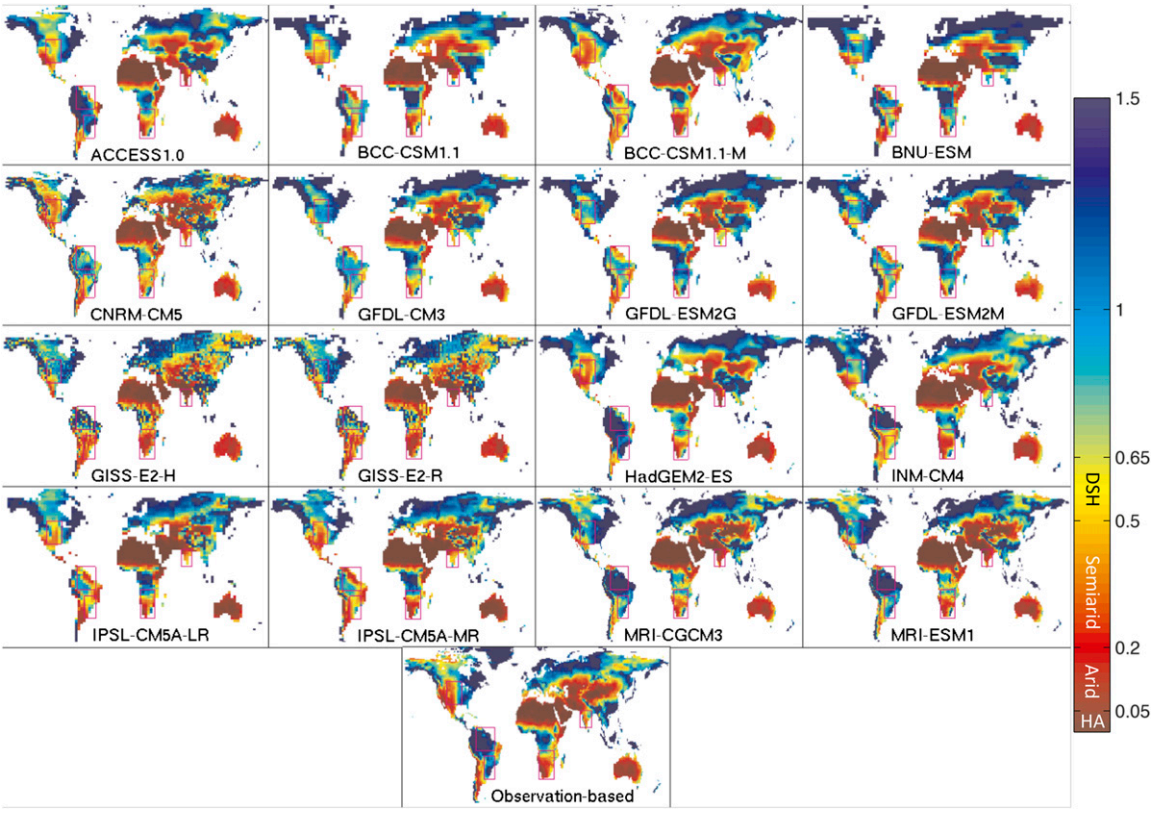

FIG. 5. 1981–99 aridity index P/PET for each model and for the observational products, where P and PET are the climatologies shown in Figs. 1 and 2. The dryland categories from Middleton and Thomas (1997) are indicated on the scale (HA = hyperarid; DSH = dry subhumid; above 0.65 is considered humid).

for the observational estimates using the nonstandard $e^* = e^*(T_{\text{mean}})$ for the monthly computations; equivalent plots for the models look similar (not shown). Thus, the discrepancies are not a simple artifact of the choice of e^* estimate. We conclude that monthly-computed PET, which does not account for the diurnal cycle of most variables or for weather variability, is not usually representative of more carefully computed climatological PET. So, we use the 3-hourly-computed PET, except where indicated.

Having examined the climatological terrestrial P and PET in the models and observations, Fig. 5 plots their ratio, the aridity index P/PET, with the UN dryland categories (Middleton and Thomas 1997) on the color scale. The large, reinforcing P and PET differences highlighted above generate similarly stark model-dependent biases in terrestrial aridity. Vast areas of South America may be simulated as anything from semiarid/arid (P/PET ~ 0.2) to extremely humid (P/PET > 1.5) depending on the model, particularly in the humid northern and southeastern regions where observed P/PET is > 1.5 and ≈ 1 respectively. The central Amazon basin, at least, is usually humid (P/PET > 0.65) in the models, but it is still much more so in some than others, again consistent with estimates for CMIP3 models in Malhi et al. (2009). There is also strong disagreement on aridity in central North America: some models depict a very large semiarid area reaching up into the central/western United States and Canada, with P/PET as low as 0.3 or so, while others keep the vast majority of the United States and Canada humid, outside of the far southwest. The observations, in contrast, have a sharp west–east gradient in aridity across the highlighted region. Similarly, the Indian subcontinent in some models is a large, nearly hyperarid desert (P/PET ≈ 0.05) similar to the Arabian Peninsula, while in others it contains regions that range from arid to humid, in line with observations. There are also interesting large-scale differences in southern to central Africa, Australia, eastern China, and many other areas. These all may be of more immediate consequence to applications than the P disagreements over tropical oceans highlighted by more general reviews such as Flato et al. (2014).

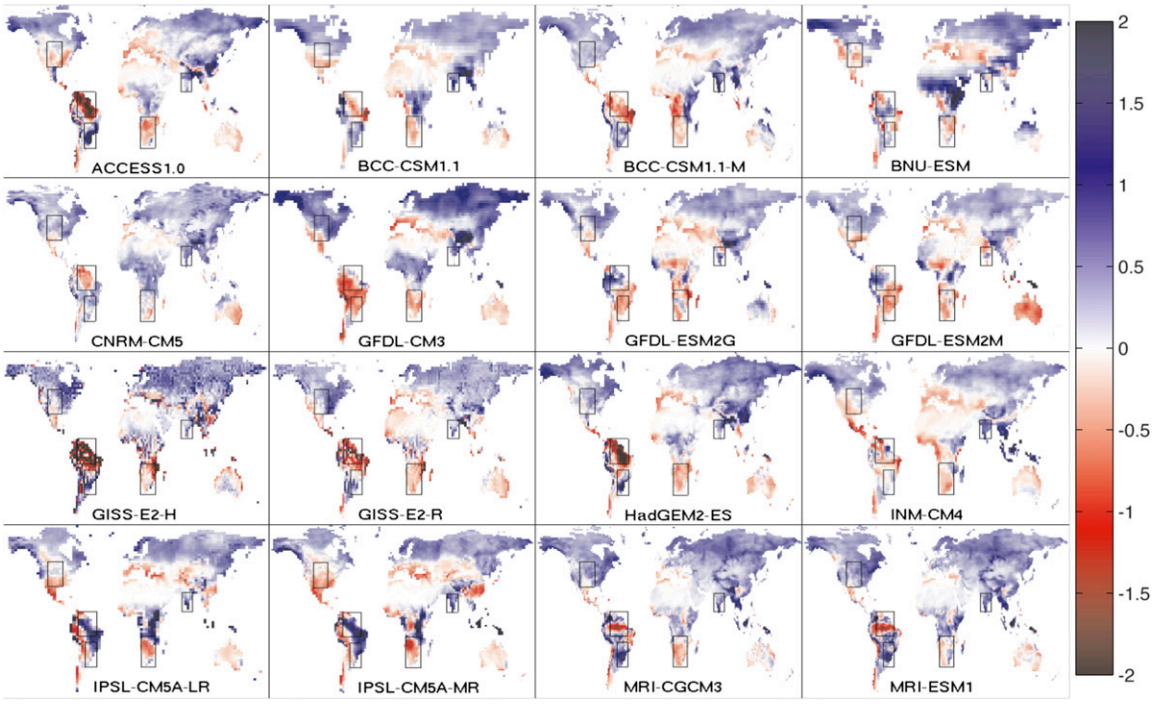

FIG. 6. Changes in annual precipitation P in mm day^{-1} between 1981–99 (historical scenario) and 2081–99 (RCP8.5 scenario), for each model.

b. Responses to greenhouse warming

Figure 6 maps the model changes in annual terrestrial P between the 1981–99 base state described above and the 2081–99 RCP8.5 future. As found in more general studies (e.g., Collins et al. 2014; Scheff and Frierson 2012a,b), P increases are generally widespread in high latitudes. However, the responses over mid- to low-latitude land do not neatly fit the typical description of deep-tropical increases and subtropical decreases found in those studies, which focused largely on P responses over the oceans because they tend to be more robust. Instead, these regions generally show patterns of both increase and decrease in P that vary widely from model to model with little zonal structure. For example, in many models the region of strongest absolute terrestrial P decline is tropical northern South America, not the subtropics. In some models (e.g., the two GFDL-ESM models) declines in P actually predominate throughout low- to midlatitude land, while in others (e.g., CNRM-CM5) increases in P predominate, with few declining regions. Most models are between these two extremes, but with widely varying, nonzonal patterns, particularly in South America, Africa, Australia, and southern to eastern Asia, and with no particular preference for P increases or decreases outside of the high latitudes.

Interestingly, these P changes do not tend to be positively related to climatological P, P/PET, or (not shown) $P - E$ across models; that is, the models that reduce P in a given location are not generally the drier ones, contrary to a "wet-get-wetter" expectation (e.g., Held and Soden 2006). For example, in northern South America HadGEM2-ES, ACCESS1.0, and the two MRI models are very humid in the mean yet have huge declines in P with greenhouse warming, and in India the two BCC and two MRI models are very arid in the mean yet show marked P increases. Figure 7 plots regional-mean change in P against basic-state P/PET to emphasize this; substantial positive correlations are absent (central North America comes closest at +0.47, although some of the driest models there still increase P the most.) All the correlation magnitudes are much less than in Fig. 3. The x axes of Fig. 7 span multiple UN aridity categories, again highlighting the zeroth-order model disagreements and biases in aridity discussed above.

In contrast, annual PET increases moderately but very robustly across all of the models and across all of global land, as shown in Fig. 8. This is just an expansion of Fig. 3 from SF14, but is shown here for reference. As shown by SF14, this is because the direct response of the Penman–Monteith equation to temperature at constant relative humidity dominates the responses to

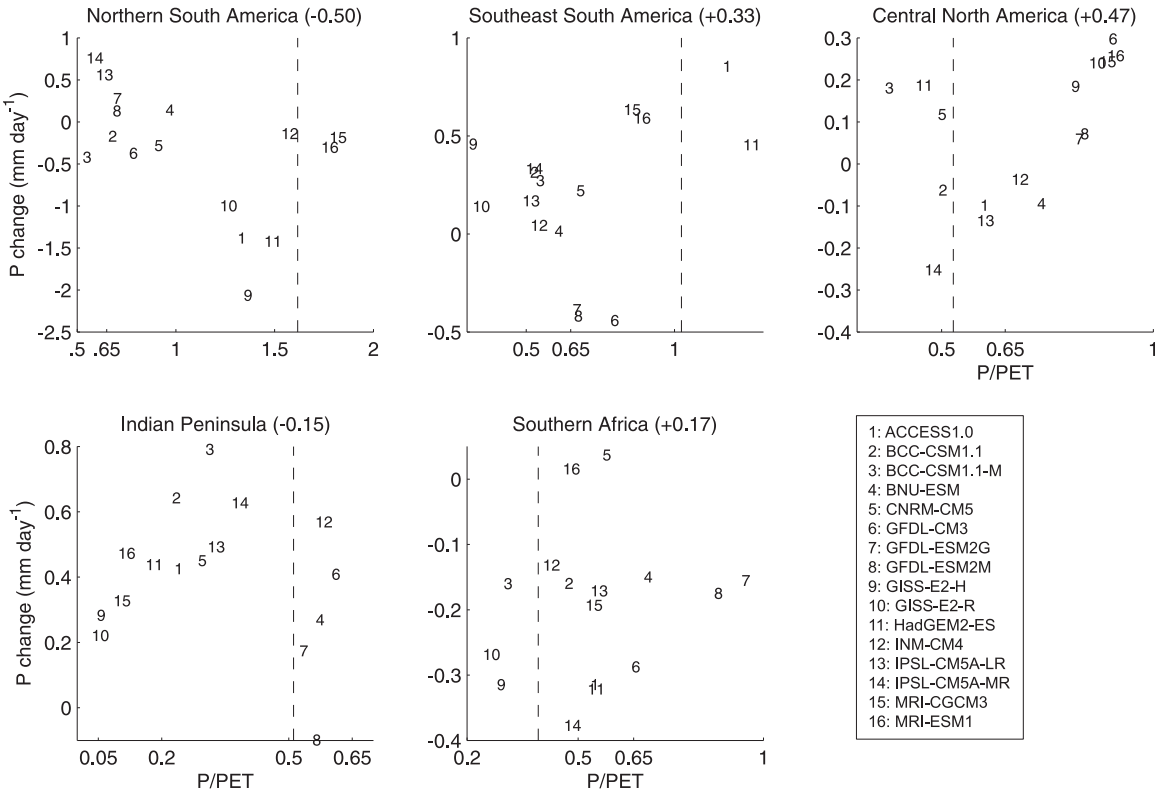

FIG. 7. Regional-land-mean 1981–99 aridity index *P*/PET vs twenty-first-century *P* change, for each model and region. Values in parentheses are simple correlations of the model points. The dashed line is observational regional-land-mean *P*/PET. For reference, *P*/PET less than 0.05 is defined as hyperarid, 0.05 to 0.2 as arid, 0.2 to 0.5 as semiarid, 0.5 to 0.65 as dry subhumid, and more than 0.65 as humid (Middleton and Thomas 1997); see the scale of Fig. 5.

the other factors, and must always be positive. The physical mechanisms for this response are the widening of the vapor pressure deficit and the increase of the equilibrium evaporative fraction, both of which come directly from the Clausius–Clapeyron equation. The percentage increases tend to be larger at higher latitudes because the percent sensitivity of (1) to temperature is much larger at cooler background temperatures, due to the lower evaporative fraction (SF14). Also, although the physical increases shown in Fig. 8 are mostly due to warming, they are much smaller than the huge, fictitious increases in PET projected by empirical temperature-based methods like the Thornthwaite equation (used in the most common version of the PDSI) and the Croley method (used in Great Lakes studies), which are clearly invalid under climate change (e.g., Hoerling et al. 2012; Lofgren et al. 2011; Hobbins et al. 2008; McKenney and Rosenberg 1993; Sheffield et al. 2012). For more details on all of this, see SF14.

Figure 9 shows the difference between the percent changes in monthly-computed PET (using the standard e^* estimate; results with the nonstandard estimate are nearly identical) and the percent changes in 3-hourly-computed PET just shown in Fig. 8. SF14 had posited that methods not explicitly resolving the diurnal cycle (such as the use of monthly output) might strongly overestimate the PET increase, because total PET is much more sensitive to conditions during the daytime, which is when greenhouse warming is generally below its diurnal average. However, with a few high-latitude exceptions in certain models, the differences (Fig. 9) are quite small compared to the increases themselves (Fig. 8), perhaps because the diurnal dependence of greenhouse warming is not actually that large outside the high latitudes (see Fig. 10.11b of Meehl et al. 2007). This lends further confidence to the results of Feng and Fu (2013), Cook et al. (2014), Dai (2013), and other studies driven by twenty-first-century changes in monthly-computed Penman–Monteith PET.

Finally, Fig. 10 maps the changes in the aridity index *P*/PET between the two epochs. The moderate, consistent Penman–Monteith PET increases (Fig. 8)

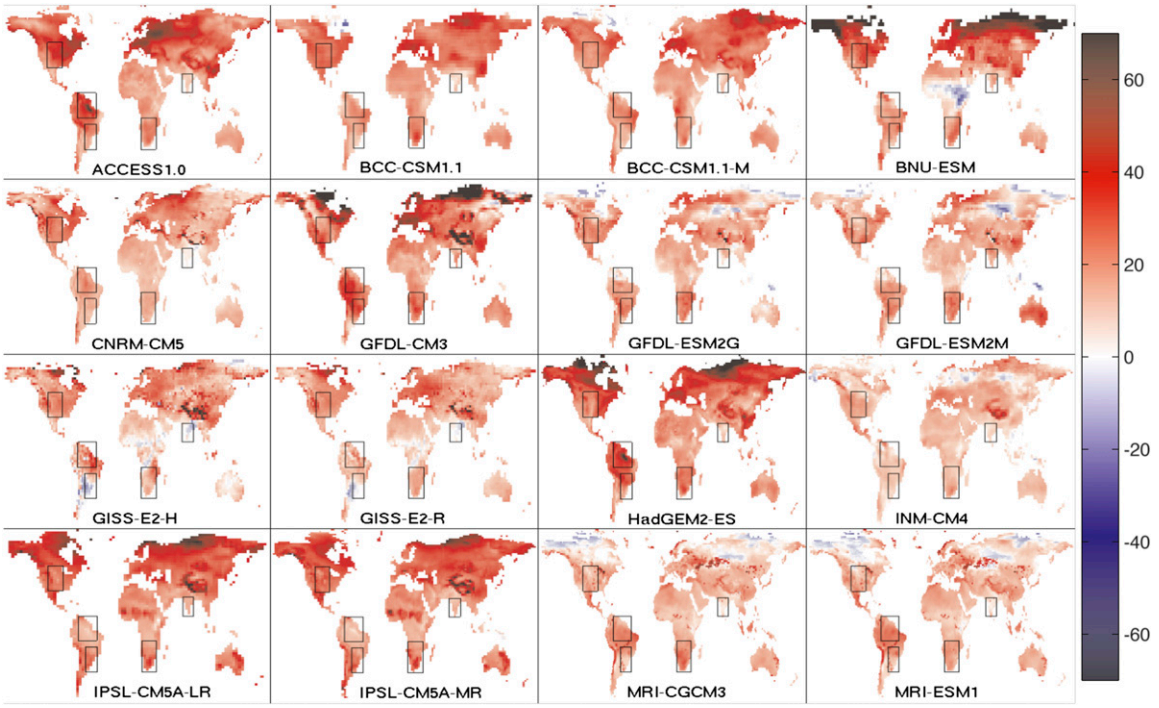

FIG. 8. Percent changes in annual PET between 1981–99 and 2081–99, for each model.

combine with the more muddled terrestrial P changes (Fig. 6) to yield widespread declines in the supply-to-demand ratio P/PET (i.e., aridification) outside of the high latitudes, with generally fewer areas of increases in P/PET. In each model, there are large areas where raw annual P (Fig. 6) increases with greenhouse warming, yet when normalized by annual PET (Fig. 10) it declines instead. Figure 10 presents a very different

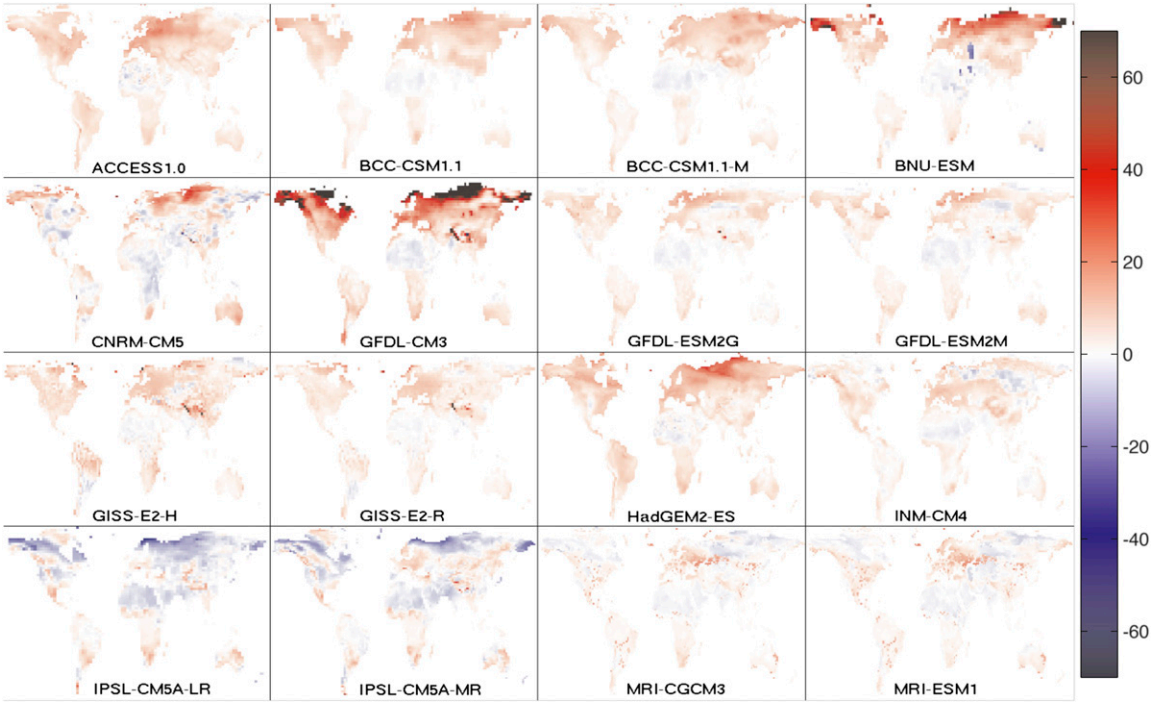

FIG. 9. Differences between the percent changes in annual PET over the twenty-first century computed using monthly vs 3-hourly output.

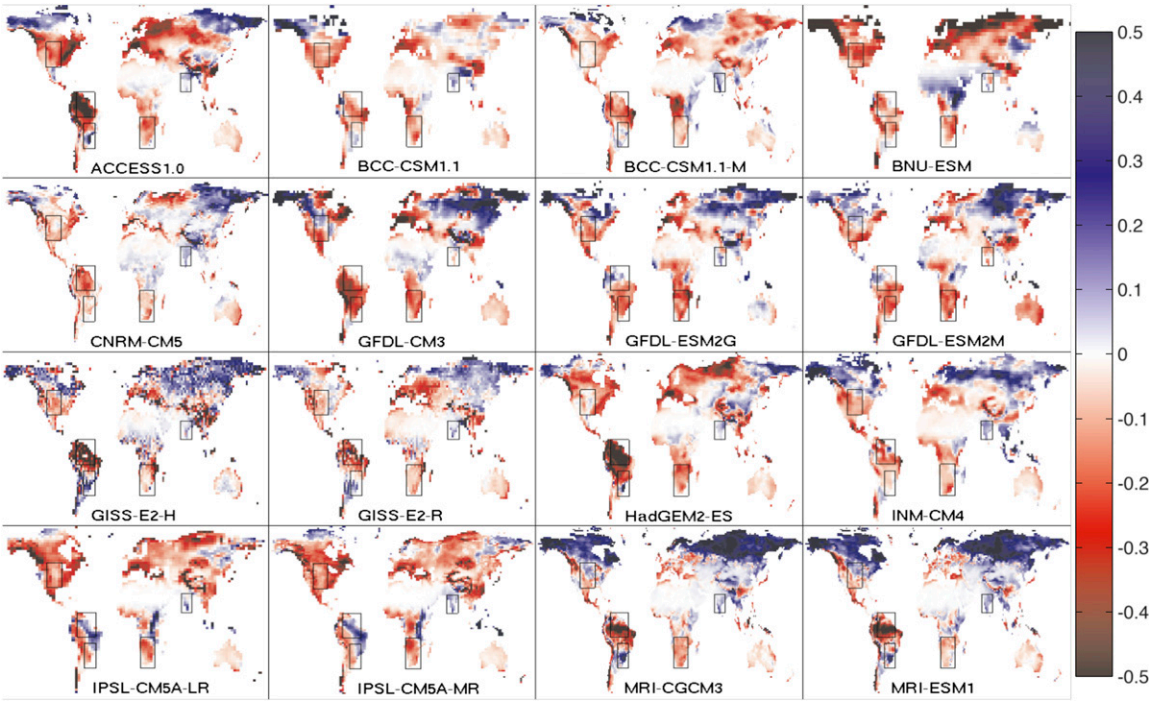

FIG. 10. Changes in the aridity index P/PET between 1981–99 and 2081–99, for each model.

story than the widespread ''wet get wetter, dry get drier'' mnemonic: terrestrial drying is dominant in the wet tropics and midlatitudes, not just in the dry subtropics.

This is the same basic picture already described by Feng and Fu (2013), Cook et al. (2014), and Dai (2013), and strongly confirms their results. However, it also has the advantages of both using a very simple, transparent aridity metric (P/PET) and showing spatial results for many different individual GCMs. In particular, one can see that some models tend to aridify more than others. Fu and Feng (2014) suggest that such global-scale disagreements on future aridity trends stem from the different phases of unforced land P variability sampled by each independent model run. However, Fig. 10 makes it clear that at least some of these differences stem from fundamental differences in the forced model response, since pairs of related models (e.g., MRI, IPSL, BCC, GFDL-ESM) look extremely similar to each other. It seems highly unlikely in light of these close similarities between independent runs that, for example, the MRI models aridify less than the others because they both happen to sample an unusually wet period of natural variation during 2081–99. Further investigation would augment this ''poor man's ensemble'' by evaluating multiple runs for each model, when possible.

4. Two alternative metrics

One disadvantage of a plot like Fig. 10, which depicts absolute changes in P/PET as in Feng and Fu (2013), is that very wet regions (e.g., the high latitudes, the Amazon, Southeast Asia) are disproportionately highlighted because the magnitude of P/PET is so much larger there already. Equivalently, as can be seen from the scale on Fig. 5, the same absolute P/PET change is much more consequential in dry climates than in wet ones: a change from 0.6 to 0.1 implies a wholesale ecoclimatic shift from subhumid savanna or forest to arid desert, while a change from 1.6 to 1.1 is merely from rather humid forest to fairly humid forest (Budyko and Miller 1974; Holdridge 1967). This makes Fig. 10 ''unfair'' in some sense. Using the reciprocal PET/P, as those older studies do, merely causes the opposite, worse problem: a change from, say, 100 to 97 in a hyperarid desert is obviously much less important than a change from 3.5 to 0.5 (semiarid to very humid.) This suggests that we might look at the *relative* changes in P/PET or PET/P, in the form of percent changes [as in Fu and Feng (2014)] or ratios [as suggested by the scale in Holdridge (1967)]. However, this still ''unfairly'' highlights tiny changes in very arid regions with $P \approx 0$: a chance increase from P/PET = 0.0001 to 0.0002 is depicted as boldly as an increase from 0.5 to 1 elsewhere, leading to rather meaningless features in

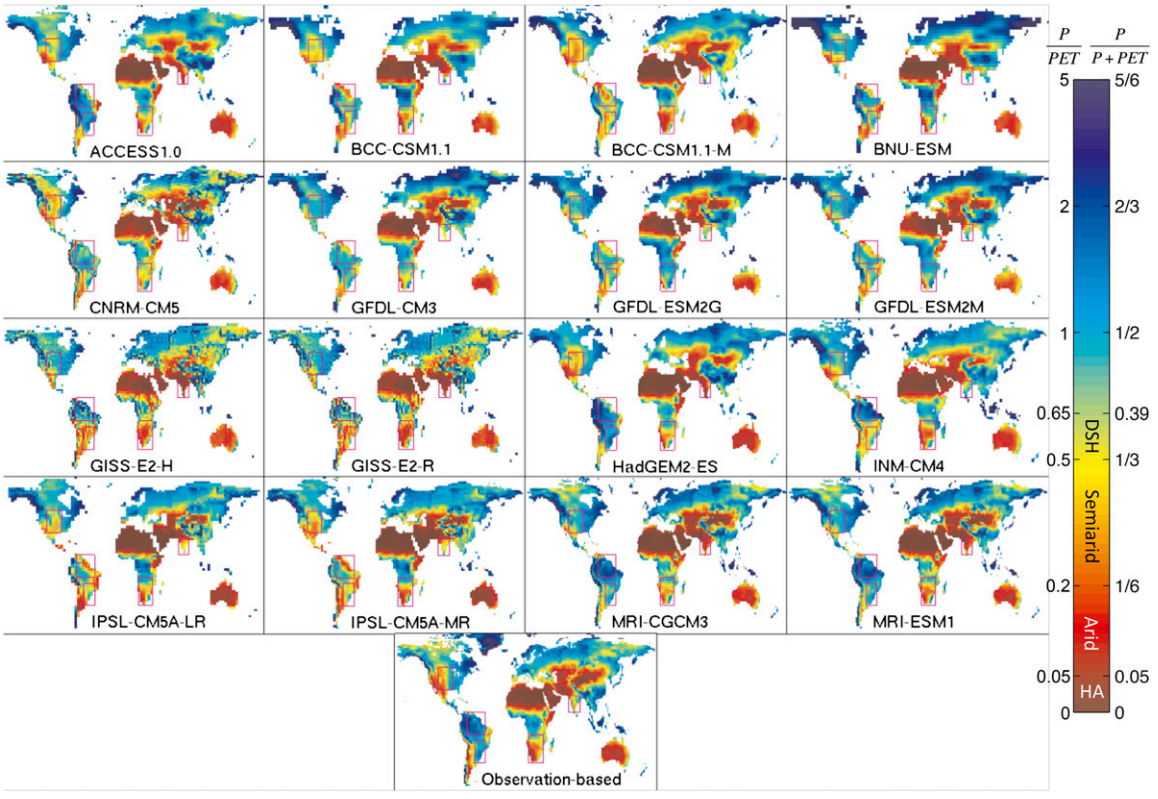

FIG. 11. 1981–99 alternate aridity index $P/(P + \text{PET})$ (right-hand scale) for each model and for the observations. The corresponding P/PET values (left-hand scale) and dryland categories are also shown for reference. Compare to Fig. 5.

places like the Sahara. [This occurs frequently in plots of percent change in P; see Fig. 12.22 of Collins et al. (2014) for examples.]

Therefore, it would be useful to employ an aridity change metric whose practical meaning does not depend so strongly on the base climate. The metrics P/PET and PET/P are each fundamentally unbalanced because they approach infinity on one side but 0 on the other. One way to portray the relative magnitudes of climatic water supply P versus demand PET in a more balanced (yet still nondimensional) fashion is to use the ratio $P/(P + \text{PET})$, which just ranges between 0 (PET $\gg P$) and 1 ($P \gg$ PET). Like the division of P and PET in the traditional index, the addition of P and PET in the denominator is not physical in and of itself but just helps us numerically assess the relative magnitudes. A similar approach is sometimes taken in terrestrial plant modeling (e.g., Medvigy et al. 2009).

Our new index $P/(P + \text{PET})$ is a one-to-one function of P/PET or PET/P,

$$\frac{P}{P + \text{PET}} = \frac{P/\text{PET}}{P/\text{PET} + 1} = \frac{1}{1 + \text{PET}/P}, \qquad (2)$$

so it preserves exactly the same information: P/PET = 1 always corresponds to $P/(P + \text{PET}) = 1/2$, P/PET = 0.2 to $P/(P + \text{PET}) = 1/6$, and so on. However, as desired, change magnitudes are not one-to-one: the above P/PET change from 0.6 to 0.1 corresponds to a $P/(P + \text{PET})$ change from 0.38 to 0.09, while the "equal" P/PET change from 1.6 to 1.1 corresponds to a $P/(P + \text{PET})$ change from just 0.62 to 0.52, nearly 3 times smaller than the first change. Essentially, P/PET = 0.6 to 0.1 represents a more dramatic change in our assessment of whether PET $\gg P$, $P \gg$ PET, or $P \sim$ PET than does P/PET = 1.6 to 1.1.

Inspired by this reasoning, Fig. 11 plots this alternate aridity index $P/(P + \text{PET})$ for each model, using the 1981–99 climatologies. As expected, it is in a one-to-one relationship with Fig. 5 (as shown on the scale), with the same spatial patterns and model-to-model differences apparent. However, the boundaries between UN dryland categories now occur at somewhat more regular intervals, and the scale is now able to saturate at more humid climates (P/PET = 5 rather than 1.5) due to the compression, allowing more information to be retained without sacrificing any detail in the drier climates. The scale also provides a handy reference for converting between the two indices.

Figure 12 then maps the changes in $P/(P + \text{PET})$ between the 2081–99 and 1981–99 periods. As desired, the

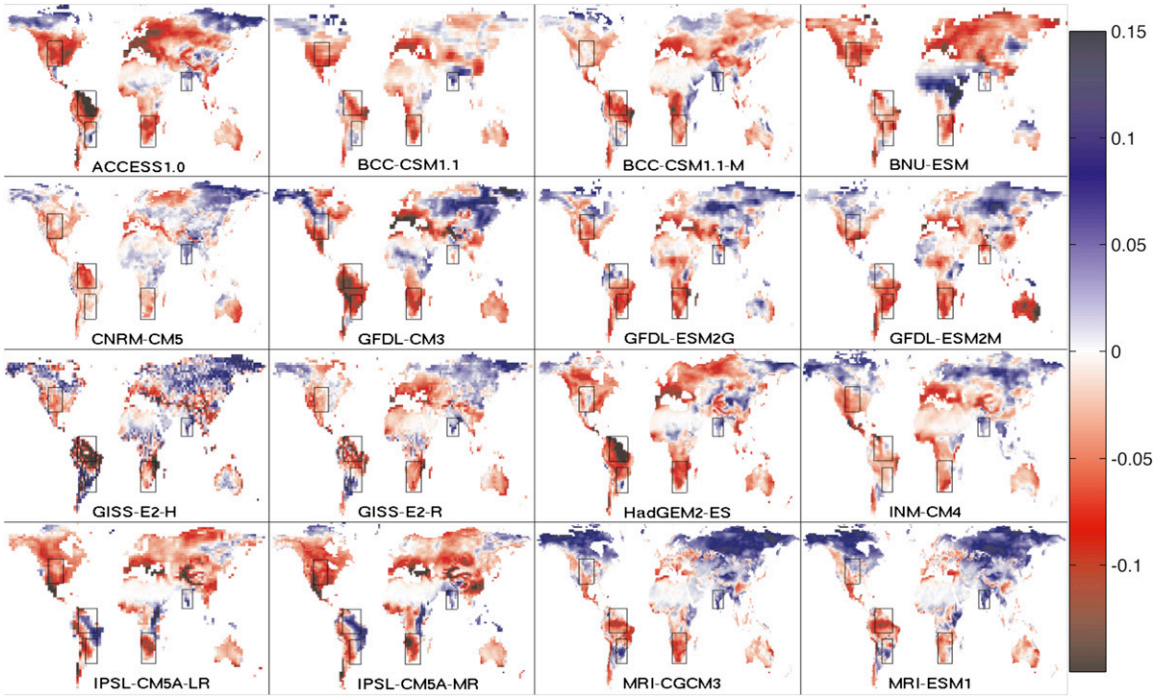

FIG. 12. Changes in the alternate aridity index $P/(P + \text{PET})$ between 1981–99 and 2081–99, for each model.

magnitudes are more spatially comparable than in Fig. 10, with high-latitude changes in particular becoming much less saturated, and subtropical changes becoming less washed out. Of course, the signs of the changes are still the same. If anything, the reduction in distracting wet-zone ''noise'' makes the overall global trend toward aridity in most models, and the fact that some models somewhat buck that trend, even clearer. The uniformly applicable scale also makes the changes more striking: everywhere that the color saturates, the modeled P versus PET balance is moving ~1/6 or more of the way from $P \gg \text{PET}$ to $\text{PET} \gg P$ or vice versa, the same as a change from semiarid to arid, or alternatively from Seattle $[P/(P + \text{PET}) = 0.53]$ to Dallas $[P/(P + \text{PET}) = 0.38]$. Aridification of this magnitude seems to occur particularly often in the Amazon, southern Europe, and Mexico and vicinity, but can happen in many diverse terrestrial locations depending on the model. Similarly, humidification of this magnitude is most commonly projected in parts of Siberia, but can also occur in parts of South America, Africa, or in subarctic North America, depending on the model. However, even the more ordinarily projected $P/(P + \text{PET})$ change magnitudes of 0.05 to 0.10 are clearly consequential on the scale of Fig. 11, and the wide prevalence of $P/(P + \text{PET})$ declines of this magnitude throughout the tropics, subtropics, and midlatitudes is a worrisome prediction.

Another common 0-to-1-valued terrestrial wetness metric is the *evaporative fraction* LH/(LH + SH) (e.g., Koster et al. 2009; Gentine et al. 2011), the proportion of total upward turbulent heat flux made up by evaporation or latent heat (LH) rather than sensible heat (SH). As with $P/(P + \text{PET})$, values closer to 1 imply more well-watered conditions, while values closer to 0 are consistent with insufficient water. The ratio LH/(LH + SH) is also an exact nonlinear function of the better-known but worse-behaved Bowen ratio SH/LH, just as $P/(P + \text{PET})$ is to PET/P. However, unlike $P/(P + \text{PET})$, the evaporative fraction is not purely a *climate* metric: LH and SH are at least proximately determined by the vegetation and soil, although their sum is constrained by the surface radiation balance. Equivalently, GCM (and GLDAS) LH and SH fields are produced by the *land* model, not by the atmospheric model (or data), and GCM land models still have great difficulty reproducing realistic LH (e.g., Sheffield et al. 2013).

However, it is still instructive to compare the two metrics. Figure 13 plots LH/(LH + SH) for each GCM and for the GLDAS, where LH and SH are 1981–99 annual means. The broad spatial patterns are quite similar to Fig. 11, with higher values in the tropics and

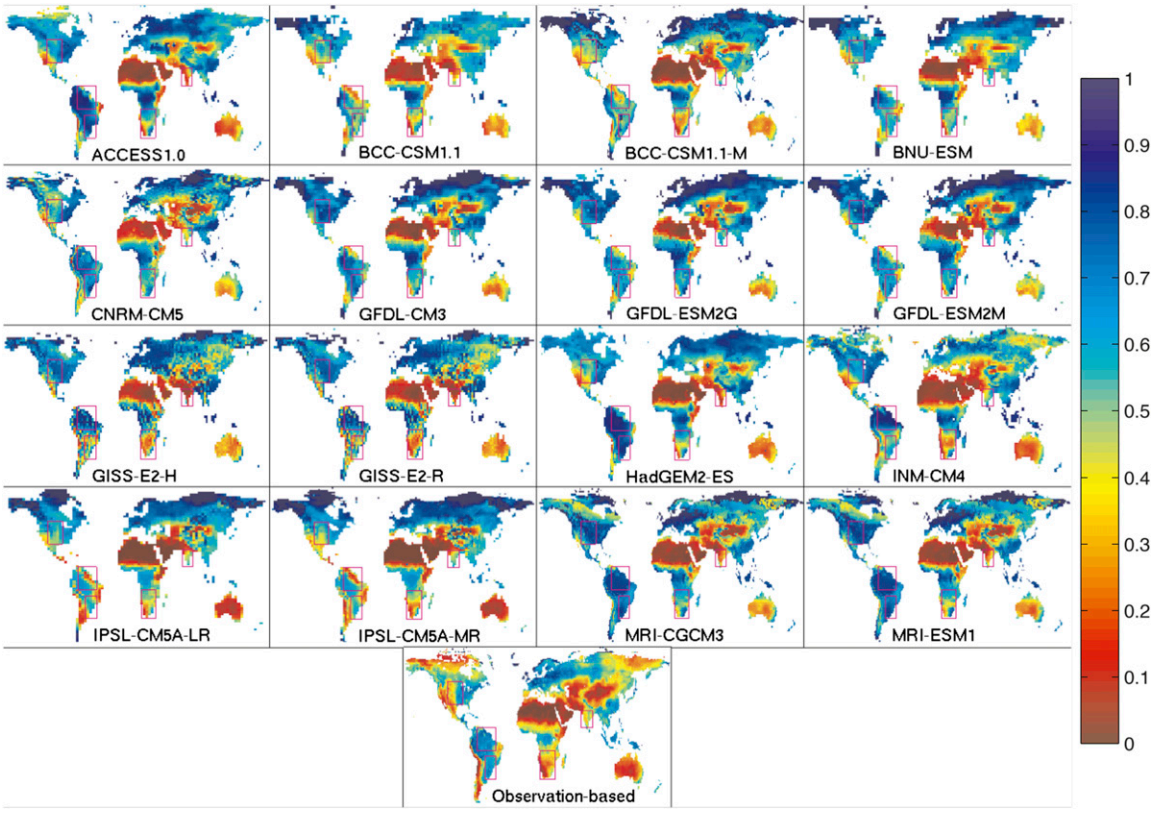

FIG. 13. 1981–99 evaporative fraction LH/(LH + SH) for each model and for the GLDAS observation-driven land model estimate.

high latitudes and lower values in the subtropical dry zones, although there is an unexplained tendency for lower LH/(LH + SH) values in GLDAS than in the GCMs, especially at higher latitudes. By plotting regional means of the two metrics against each other, Fig. 14 shows that $P/(P + \text{PET})$ and LH/(LH + SH) also agree extremely well on which GCMs are drier versus wetter in a given location; the correlations are always at least +0.89. This reassuringly implies that the GCM land models are consistently responding to climate forcing, though the unusually low LH/(LH + SH) values in GLDAS for a given $P/(P + \text{PET})$ are still apparent.

Will greenhouse warming responses of LH/(LH + SH) also follow greenhouse warming responses of $P/(P + \text{PET})$? One might not expect so, since for a constant surface-wetness state, LH/(LH + SH) fundamentally increases with warming due to the Clausius–Clapeyron equation (e.g., Hartmann 1994). For example, LH/(LH + SH) is much higher over tropical oceans than over high-latitude oceans, even though they are equally "wet." This could offset some of the expected drying-induced declines in LH/(LH + SH). Indeed, Fig. 15 shows that unlike $P/(P + \text{PET})$ in Fig. 12, LH/(LH + SH) variously increases or decreases with projected warming in the GCMs, with no clear sign preference. However, this neutrality still implies drying with warming, since warming *alone* (without any surface drying) would lead to systematic *increases* in LH/(LH + SH) as explained above. Also, the geographic patterns of the responses in Figs. 12 and 15 appear quite similar, although the signs may be different. Figure 16 shows that regional intermodel disagreements are also very consistent between $P/(P + \text{PET})$ responses and LH/(LH + SH) responses, just as they were for the metrics' mean states; intermodel correlations are at least +0.86 in each region. Thus, in GCMs, the atmosphere/hydroclimate response to greenhouse warming seems very relevant for the land hydrologic response, increasing our confidence in the land models.

5. Summary and conclusions

The aridity of a terrestrial climate is generally quantified using the relative magnitudes of precipitation P and potential evapotranspiration PET. This study evaluates the climatologies and greenhouse-warming responses of terrestrial P, Penman–Monteith PET (1),

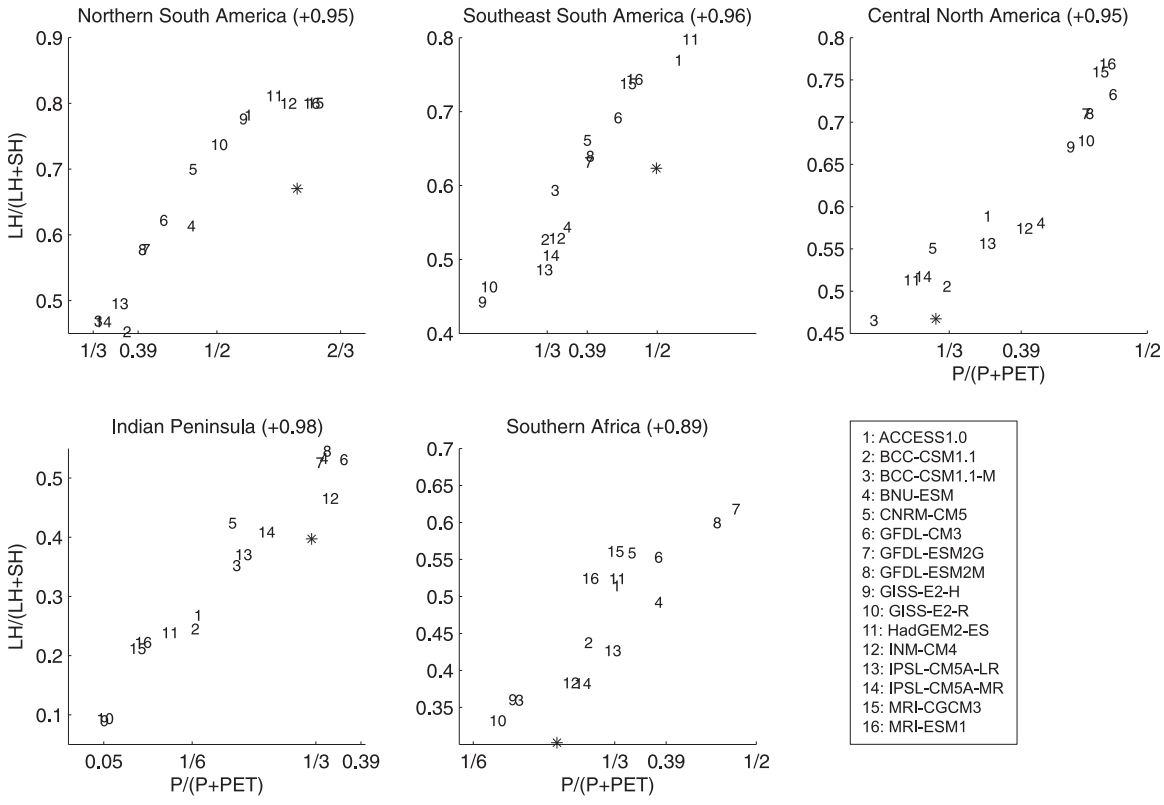

FIG. 14. 1981–99 regional-land-mean alternate aridity index $P/(P + \mathrm{PET})$ vs evaporative fraction $\mathrm{LH}/(\mathrm{LH} + \mathrm{SH})$ for each model (numbers) and for the observational products (asterisks), for each region. Values in parentheses are simple correlations of the 16 model points. For reference, $P/(P + \mathrm{PET})$ less than ≈ 0.05 is defined as hyperarid, ≈ 0.05 to $1/6$ as arid, $1/6$ to $1/3$ as semiarid, $1/3$ to ≈ 0.39 as dry subhumid, and more than ≈ 0.39 as humid; see the scale of Fig. 11.

and their dimensionless ratio P/PET (the *aridity index*) in 16 different CMIP5 global climate models. The climatologies generally agree in much of Eurasia and North Africa, but they disagree dramatically in large areas of the Americas, sub-Saharan Africa, South Asia, and elsewhere, with the same areas represented as semiarid-to-arid or quite humid by different models (Figs. 1, 2, 3, 5, and 7). In many of these areas, P and PET are much closer to the observations in some models than in others, and PET is often high in the same models for which P is low, strengthening the P/PET disagreements and biases.

The terrestrial P responses to warming tend to be positive at high latitudes, but an inconsistent and complex mixture of positive and negative elsewhere, counter to both naive expectations of more P in a warmer climate and ocean-inspired theories of strongly zonal P response to warming (Fig. 6). Since the Penman–Monteith PET responses to warming are uniformly and substantially positive in contrast (SF14 and Fig. 8), aridification (P/PET decline) generally dominates over humidification (P/PET increase) in the tropics, the subtropics, and the midlatitudes (Fig. 10), with varying spatial patterns. This is in marked contrast to the expectation from a "wet get wetter, dry get drier" rule, but strongly agrees with more recent studies (Dai 2013; Feng and Fu 2013; Cook et al. 2014). However, this global drying tendency is much less apparent in certain models.

The PET climatologies are also found to be sensitive to the computation time scale: except at high latitudes, the aerodynamic (right-hand) part of (1) is uniformly 20%–50% higher when computed using monthly rather than 3-hourly GCM output, making total PET 10%–30% higher in large areas (Fig. 4). However, contrary to the authors' earlier suggestion (SF14), the responses to greenhouse warming are not as sensitive to this choice of input time scale, though there are large local differences in some models (Fig. 9). The use of diurnally averaged temperature to estimate the monthly-mean saturation vapor pressure e^* (as done by the above studies, counter to standard procedure) does not change the general magnitude of any of these comparisons, though the details for the climatologies differ.

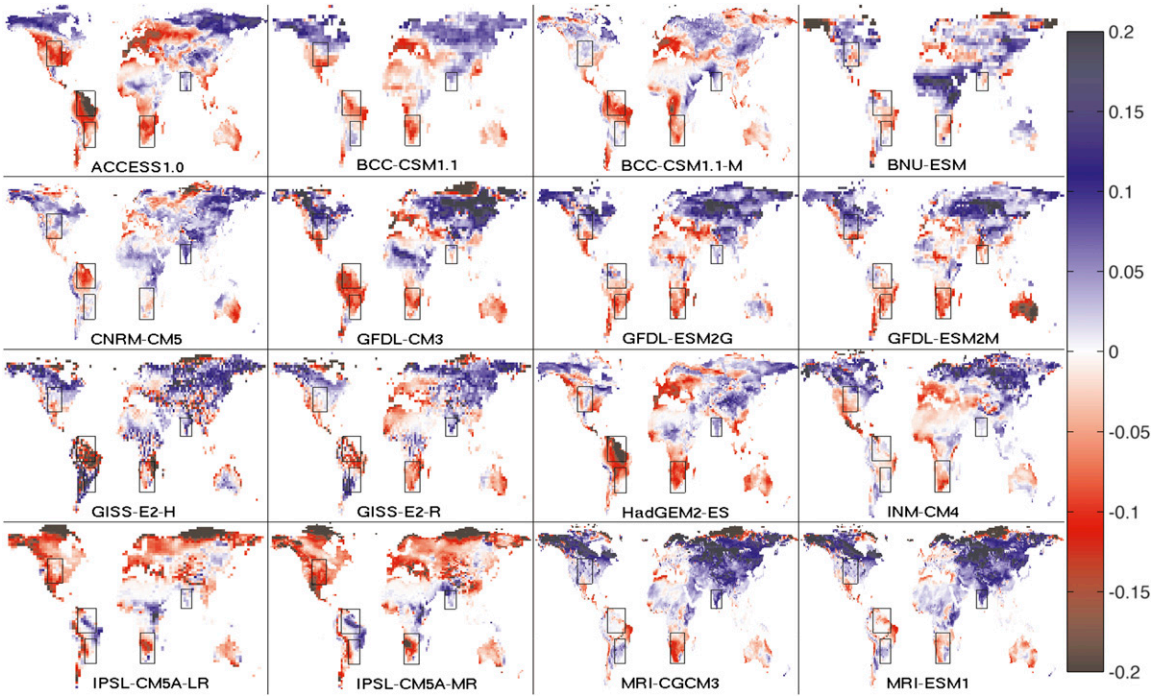

FIG. 15. Changes in evaporative fraction LH/(LH + SH) between 1981–99 and 2081–99, for each model.

The same change in P/PET is much more meaningful when P/PET is low than when it is high. Therefore, an alternative index $P/(P + \text{PET})$ (Fig. 11), which carries the same information as P/PET but only varies from 0 (PET $\gg P$) to 1 ($P \gg$ PET), is also used to quantify the model aridities and responses to warming. Indeed, the responses of $P/(P + \text{PET})$ (Fig. 12) are more spatially comparable than those of P/PET (Fig. 10), with a more uniform interpretation. This alternative method better highlights aridity changes in all terrestrial regions, rather than disproportionately focusing on changes in wet or very dry places. These $P/(P + \text{PET})$ climatologies and changes are also consistent in many ways with evaporative fraction [LH/(LH + SH)] climatologies and changes (Figs. 13–16), though the latter are fundamentally biased positive by the warming itself apart from any water-availability change, obscuring the aridity-related signal (Fig. 15).

One problem with this study, and with all the cited studies that use PET to think about the terrestrial response to greenhouse warming, is that PET is just a notional flux: it is never actually realized, except in irrigated or very humid settings. The authors are in the process of developing a new framework for thinking about the effect of warming when actual ET < PET. Preliminary results suggest that if the actual evaporative fraction is much less than the notional evaporative fraction from a wet surface, then the actual ET requirement for plants will have a *higher* percentage sensitivity to warming than will PET, because it will be less energetically constrained. Thus, the warming/drying result may become even stronger in this framework. However, it is also important to note that ambient carbon dioxide increases might reduce plant ET requirements (e.g., Sellers et al. 1996), introducing the opposite effect. Much more work needs to be done.

Finally, it is often suggested in the paleoclimate literature that warm greenhouse climates of the past are well watered and cold climates such as the last glacial maximum are arid, contrary to the conclusions above. Could model biases, either in land parameterizations or atmospheric physics parameterizations, be exaggerating the global drying tendency? The authors have work planned and in progress attempting to reconcile these perspectives with a combination of paleoclimate model analysis, moisture proxy meta-analysis, and idealized climate modeling. The resolution of this dilemma could greatly improve our understanding of the future of terrestrial aridity.

Acknowledgments. We acknowledge the World Climate Research Programme's Working Group on Coupled Modelling, which is responsible for CMIP, and we thank the climate modeling groups (listed in Table 1 of this paper) for producing and making available their

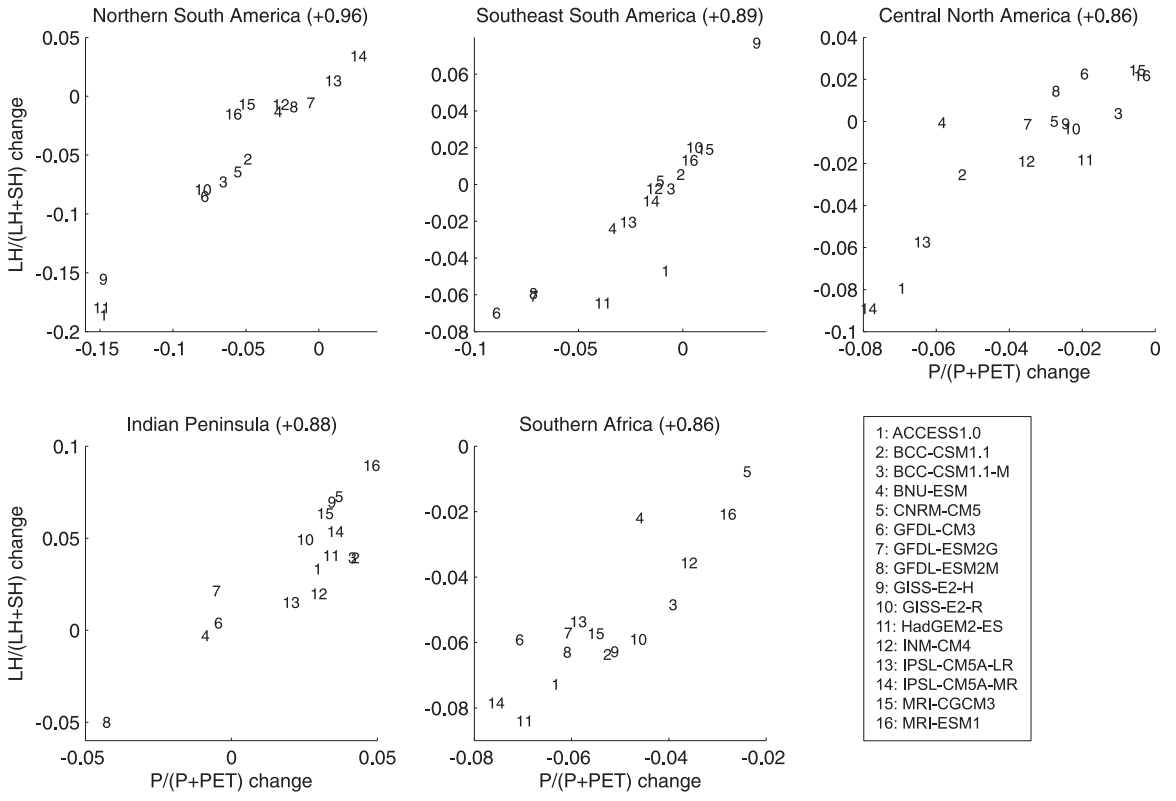

FIG. 16. Regional-land-mean twenty-first-century $P/(P + \text{PET})$ change vs LH/(LH + SH) change, for each model and region. Values in parentheses are simple correlations of the model points.

model output. For CMIP the U.S. Department of Energy's Program for Climate Model Diagnosis and Intercomparison provides coordinating support and led development of software infrastructure in partnership with the Global Organization for Earth System Science Portals. J. S. would also like to thank the two anonymous reviewers for suggestions that greatly strengthened this paper. This work was supported by NSF Awards AGS-0846641, AGS-0936059, AGS-1359464, AGS-1433551, and PLR-1341497.

REFERENCES

Allen, R. G., L. S. Pereira, D. Raes, and M. Smith, 1998: Crop evapotranspiration: Guidelines for computing crop water requirements. FAO Irrigation and Drainage Paper 56, 174 pp. [Available online at http://www.fao.org/docrep/x0490e/x0490e00.htm.]

——, I. A. Walter, R. Elliott, T. Howell, D. Itenfisu, and M. Jensen, 2005: The ASCE standardized reference evapotranspiration equation. American Society of Civil Engineers, 59 pp. [Available online at http://www.kimberly.uidaho.edu/water/asceewri/ascestzdetmain2005.pdf.]

Brutsaert, W., and M. B. Parlange, 1998: Hydrologic cycle explains the evaporation paradox. *Nature,* **396,** 30, doi:10.1038/23845.

Budyko, M. I., and D. H. Miller, 1974: *Climate and Life.* International Geophysics Series, Vol. 18, Academic Press, 508 pp.

Collins, M., and Coauthors, 2014: Long-term climate change: Projections, commitments and irreversibility. *Climate Change 2013: The Physical Science Basis,* T. F. Stocker et al., Eds., Cambridge University Press, 1029–1136.

Cook, B. I., J. E. Smerdon, R. Seager, and S. Coats, 2014: Global warming and 21st century drying. *Climate Dyn.,* **43,** 2607–2627, doi:10.1007/s00382-014-2075-y.

Dai, A., 2013: Increasing drought under global warming in observations and models. *Nat. Climate Change,* **3,** 52–58, doi:10.1038/nclimate1633.

Feng, S., and Q. Fu, 2013: Expansion of global drylands under a warming climate. *Atmos. Chem. Phys.,* **13,** 10 081–10 094, doi:10.5194/acp-13-10081-2013.

Flato, G., and Coauthors, 2014: Evaluation of climate models. *Climate Change 2013: The Physical Science Basis,* T. F. Stocker et al., Eds., Cambridge University Press, 741–866.

FAO, 2004: Global map of monthly reference evapotranspiration—10 arc minutes. Food and Agriculture Organization. Accessed 7 June 2015. [Available online at http://www.fao.org/geonetwork/srv/en/metadata.show?id=7416&currTab=distribution.]

Fu, Q., and S. Feng, 2014: Responses of terrestrial aridity to global warming. *J. Geophys. Res. Atmos.,* **119,** 7863–7875, doi:10.1002/2014JD021608.

Gentine, P., D. Entekhabi, and J. Polcher, 2011: The diurnal behavior of evaporative fraction in the soil–vegetation–atmospheric

boundary layer continuum. *J. Hydrometeor.,* **12,** 1530–1546, doi:10.1175/2011JHM1261.1.

Harris, I., P. D. Jones, T. J. Osborn, and D. H. Lister, 2014: Updated high-resolution grids of monthly climatic observations—The CRU TS3.10 dataset. *Int. J. Climatol.,* **34,** 623–642, doi:10.1002/joc.3711.

Hartmann, D., 1994: *Global Physical Climatology.* International Geophysics Series, Vol. 56, Academic Press, 411 pp.

Held, I., and B. Soden, 2006: Robust responses of the hydrological cycle to global warming. *J. Climate,* **19,** 5686–5699, doi:10.1175/JCLI3990.1.

Hobbins, M. T., A. Dai, M. L. Roderick, and G. D. Farquhar, 2008: Revisiting the parameterization of potential evaporation as a driver of long-term water balance trends. *Geophys. Res. Lett.,* **35,** L12403, doi:10.1029/2008GL033840.

Hoerling, M. P., J. K. Eischeid, X.-W. Quan, H. F. Diaz, R. S. Webb, R. M. Dole, and D. R. Easterling, 2012: Is a transition to semipermanent drought conditions imminent in the U.S. Great Plains? *J. Climate,* **25,** 8380–8386, doi:10.1175/JCLI-D-12-00449.1.

Holdridge, L. R., 1967: *Life Zone Ecology.* Tropical Science Center, 206 pp.

Koster, R. D., S. D. Schubert, and M. J. Suarez, 2009: Analyzing the concurrence of meteorological droughts and warm periods, with implications for the determination of evaporative regime. *J. Climate,* **22,** 3331–3341, doi:10.1175/2008JCLI2718.1.

Lofgren, B. M., T. S. Hunter, and J. Wilbarger, 2011: Effects of using air temperature as a proxy for potential evapotranspiration in climate change scenarios of Great Lakes basin hydrology. *J. Great Lakes Res.,* **37,** 744–752, doi:10.1016/j.jglr.2011.09.006.

Malhi, Y., and Coauthors, 2009: Exploring the likelihood and mechanism of a climate-change-induced dieback of the Amazon rainforest. *Proc. Natl. Acad. Sci. USA,* **106,** 20 610–20 615, doi:10.1073/pnas.0804619106.

McKenney, M. S., and N. J. Rosenberg, 1993: Sensitivity of some potential evapotranspiration estimation methods to climate change. *Agric. For. Meteor.,* **64,** 81–110, doi:10.1016/0168-1923(93)90095-Y.

Medvigy, D., S. C. Wofsy, J. W. Munger, D. Y. Hollinger, and P. R. Moorcroft, 2009: Mechanistic scaling of ecosystem function and dynamics in space and time: Ecosystem Demography model version 2. *J. Geophys. Res.,* **114,** G01002, doi:10.1029/2008JG000812.

Meehl, G. A., and Coauthors, 2007: Global climate projections. *Climate Change 2007: The Physical Science Basis,* S. Solomon et al., Eds., Cambridge University Press, 747–845.

Middleton, N., and D. S. G. Thomas, 1997: *World Atlas of Desertification.* 2nd ed. Wiley, 182 pp.

Milly, P. C. D., 1992: Potential evaporation and soil moisture in general circulation models. *J. Climate,* **5,** 209–226, doi:10.1175/1520-0442(1992)005<0209:PEASMI>2.0.CO;2.

Monteith, J. L., 1981: Evaporation and surface temperature. *Quart. J. Roy. Meteor. Soc.,* **107,** 1–27, doi:10.1002/qj.49710745102.

Mortimore, M., and Coauthors, 2009: Dryland opportunities: A new paradigm for people, ecosystems and development. IUCN, IIED, and UNDP/DDC Challenge Paper, 86 pp. [Available online at http://pubs.iied.org/pdfs/G02572.pdf.]

Rodell, M., and Coauthors, 2004: The Global Land Data Assimilation System. *Bull. Amer. Meteor. Soc.,* **85,** 381–394, doi:10.1175/BAMS-85-3-381.

Scheff, J., and D. M. W. Frierson, 2012a: Twenty-first-century multimodel subtropical precipitation declines are mostly midlatitude shifts. *J. Climate,* **25,** 4330–4347, doi:10.1175/JCLI-D-11-00393.1.

——, and ——, 2012b: Robust future precipitation declines in CMIP5 largely reflect the poleward expansion of model subtropical dry zones. *Geophys. Res. Lett.,* **39,** L18704, doi:10.1029/2012GL052910.

——, and ——, 2014: Scaling potential evapotranspiration with greenhouse warming. *J. Climate,* **27,** 1539–1558, doi:10.1175/JCLI-D-13-00233.1.

Schneider, U., A. Becker, P. Finger, A. Meyer-Christoffer, M. Ziese, and B. Rudolf, 2014: GPCC's new land surface precipitation climatology based on quality-controlled in situ data and its role in quantifying the global water cycle. *Theor. Appl. Climatol.,* **115,** 15–40, doi:10.1007/s00704-013-0860-x.

Sellers, P., and Coauthors, 1996: Comparison of radiative and physiological effects of doubled atmospheric CO_2 on climate. *Science,* **271,** 1402–1406, doi:10.1126/science.271.5254.1402.

Sheffield, J., G. Goteti, and E. F. Wood, 2006: Development of a 50-year high-resolution global dataset of meteorological forcings for land surface modeling. *J. Climate,* **19,** 3088–3111, doi:10.1175/JCLI3790.1.

——, E. F. Wood, and M. L. Roderick, 2012: Little change in global drought over the past 60 years. *Nature,* **491,** 435–438, doi:10.1038/nature11575.

——, and Coauthors, 2013: North American climate in CMIP5 experiments. Part I: Evaluation of historical simulations of continental and regional climatology. *J. Climate,* **26,** 9209–9245, doi:10.1175/JCLI-D-12-00592.1.

Taylor, K. E., R. J. Stouffer, and G. A. Meehl, 2012: An overview of CMIP5 and the experiment design. *Bull. Amer. Meteor. Soc.,* **93,** 485–498, doi:10.1175/BAMS-D-11-00094.1.

Transeau, E. N., 1905: Forest centers of eastern America. *Amer. Nat.,* **39,** 875–889, doi:10.1086/278586.